Terra Antartica
2001, 8(3), 197-204

Stress Patterns Observed by Borehole Televiewer Logging of the CRP-3 Drillhole, Victoria Land Basin, Antarctica

R.D. JARRARD[1*], D. MOOS[2], T.J. WILSON[3], C.J. BÜCKER[4,§] & T.S. PAULSEN[5]

[1]Dept. of Geology & Geophysics, 717 WBB, Univ. of Utah, 135 S. 1460 East, Salt Lake City UT 84112-0111 - U.S.A.
[2]Dept. of Geophysics, Stanford University, Stanford, CA 94305-2215 - U.S.A.
[3]Dept. of Geological Sciences, Ohio State University, 275 Mendenhall, 125 S. Oval Mall, Columbus OH 43210 - U.S.A.
[4]GGA, Leibniz Institute for Applied Geosciences, Stilleweg 2, 30655 Hannover - Germany
[5]Dept. of Geology, University of Wisconsin, 800 Algoma Blvd., Oshkosh, WI 54901 - U.S.A.
[§]Present address: RWE-DEA AG, Ueberseering 40, 22297 Hamburg - Germany

Received 28 October 2000; *accepted in revised form* 6 December 2001

Abstract - Borehole televiewer logs were recorded over 92% of the CRP-3 drillhole. Processed televiewer images detect a variety of features in the borehole wall, including bedding, lonestones, conglomerates, fractures, and breakouts. Data quality varied from poor in much of the top 350 mbsf to excellent in the lower portion of the hole. Three types of stress-induced drillhole failures - breakouts, petal centre-line fractures, and tensile fractures - were analyzed to determine the present-day stress state. Using the elastic equations for stress concentrations around a borehole, we estimate stress magnitudes and conclude that the stress state within CRP-3 is strike-slip. The minimum horizontal stress direction is N75°E ± 6° (N70°E ± 6° for breakouts, the most accurate stress indicators). This average direction agrees with the N77°E direction of minimum horizontal stress determined from CRP-2A televiewer data. Both stress directions exclude topography as a possible control on local horizontal stresses, as topographic effects would generate a minimum horizontal stress direction of S82°E. In contrast, the modern minimum stress direction is similar to the extension direction that caused faulting and related structural dips toward N70°E ± 5°.

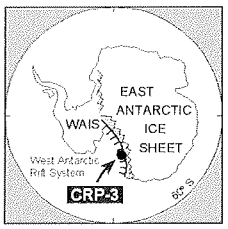

INTRODUCTION

The World Stress Map (Zoback, 1992) is not truly global in its coverage, because virtually no data are available from the interior of the Antarctic plate. The majority of World Stress Map data are focal mechanisms, but Antarctica lacks both large earthquakes and local seismic networks capable of detecting smaller earthquakes. Furthermore, many (28%) of the stress directions shown on the World Stress Map are derived from borehole breakouts, borehole enlargements caused by compressive failure of the sides of a drillhole. Within the Antarctic plate, however, there have been no industry drillholes and only a handful of scientific drillholes, none of which has detected breakouts. This paucity of stress directions hampers studies of driving forces based on intraplate stress data (*e.g.*, Richardson, 1992), as the Antarctic plate is one of only two plates that are surrounded by ridges.

An opportunity to determine stress directions within part of the Antarctic plate is provided by the Cape Roberts Project (CRP). CRP is an international drilling project whose aim is to reconstruct Neogene to Palaeogene palaeoclimate and the tectonic history of the Transantarctic Mountains and West Antarctic rift system, by obtaining continuous cores and well logs from a site near Cape Roberts, Antarctica. Offshore Cape Roberts, tilting and erosion of strata have brought Lower Miocene to Lower Oligocene sediments near the seafloor. The three CRP holes penetrate successively older portions of a 1600 m composite stratigraphic sequence. The third CRP drillhole, CRP-3, cored 821 m of Lower Oligocene and possibly Upper Eocene sedimentary rocks and 116 m of underlying Devonian sandstone (Cape Roberts Science Team, 2000). Average core recovery was 97%. The mid-Tertiary section consists primarily of sandstones and muddy sandstones; other lithologies include common thin conglomerate beds and less common sandy mudstones and diamictites (Cape Roberts Science Team, 2000).

Moos et al. (2000) analyzed borehole televiewer (BHTV) logs from the second CRP drillhole, CRP-2/2A, and utilized the results both to determine the direction of minimum horizontal stress and to provide bounds on the overall stress state. This paper undertakes a similar analysis for CRP-3 based on its BHTV log.

*Corresponding author (jarrard@mail.mines.utah.edu)

METHODS

DATA ACQUISITION AND PROCESSING

BHTV well logging was undertaken during three phases of the drilling of CRP-3. The first phase was at the conclusion of drilling with HQ drillrod (102-mm diameter), and the next two phases were midway and at the conclusion of NQ (80-mm diameter) drilling. The BHTV is an acoustic instrument that provides an image of surface reflectivity of the wall of a fluid-filled borehole (Zemanek et al., 1970). An acoustic transducer in the tool fires a sound pulse, which travels through the borehole fluid, bounces off the borehole wall, and returns to the transducer. The Antares® BHTV used at CRP-3 is a digital tool which analyzes the received waveform from each transducer pulse, picks amplitude and traveltime of the reflection from the borehole wall, and transmits these values to the surface electronics in real time. The transducer, which is mounted on a rotating shaft, sends and receives either 72 or 144 pulses per rotation. As the tool is pulled up the hole, the rotating transducer obtains continuous 360° images of both amplitude and traveltime. The logging speed of 1.2 m/min results in a vertical resolution of 3 mm. Reflection amplitude depends mainly on reflectivity and roughness of the borehole wall. Traveltime depends on the diameter of the borehole.

The BHTV logging tool includes two accelerometers and three perpendicular magnetometers, for tool orientation. The CRP-3 accelerometer logs indicated that hole deviation was minor, less than 2.5° from vertical (Cape Roberts Science Team, 2000). The two horizontal magnetometers provide a continuous record of orientation of the tool with respect to magnetic north, so that all images can be converted from tool coordinates to magnetic north. We converted the images from magnetic north to true north coordinates, using measurements of local deviation based on an on-ice reference magnetometer. The CRP-3 site is actually at a higher latitude than the South Magnetic Pole, and it is so close to the magnetic pole that we considered it necessary to test the 148° (S32°E) local deviation based on the International Geomagnetic Reference Field (IGRF). An additional concern at very high latitudes is that magnetic storms can cause sudden, large swings in local deviation. Consequently, the reference magnetometer recorded 3-component magnetic field direction throughout BHTV logging. Fortunately, magnetic storm activity was minor during logging, causing declination variations of <3°. Our measurements with the reference magnetometer were consistent with the IGRF value: 147-148°. All BHTV images were oriented to true north with corrections for both average and time-varying local deviation.

BHTV logs were obtained for 92% of CRP-3. Two intervals were not logged because hole conditions were too unstable to risk losing the tool: the upper fault zone (255.1-271.4 mbsf), and the bottom part of the hole (898.5-939 mbsf), which was blocked by swelling clays in an altered intrusion. Log quality varied from poor to excellent, generally improving with increasing depth. Much of the top half of the BHTV log provided only rare returns from the borehole wall, possibly because of mudcake. It was usually possible, however, to identify enough features in this upper log to orient cores (Jarrard, Paulsen & Wilson, this volume). All of the raw BHTV images exhibited vertical striping that partially masked geologically meaningful features. This striping was removed by preprocessing, and then images were displayed with false colors to enhance subtle features.

The amplitude images were most useful for identification of geologic features such as fractures, bedding, and clasts. The CRP-3 traveltime logs did not provide reliable measurements of hole size, because of a combination of poor calibration by Antares® and cycle skipping. They occasionally provided useful images of borehole features, particularly open fractures and clasts, but these features generally were imaged as well or better by the amplitude log. Hole size was quite uniform, based on dipmeter measurements (Cape Roberts Science Team, 2000).

The CRP-3 BHTV logs, like other CRP-3 well logs, exhibited up to 2.5 m of depth shift compared to coring depths, caused mainly by stretch of the logging cable. This shift varied both between and within logging runs. We corrected the BHTV data to minimize depth shifts, based on identification of depths of 337 correlative features on the core logs (Cape Roberts Science Team, 2000) and BHTV images. Optimum depth shift for each of 11 intervals of BHTV log was calculated. The final shifted logs have residual depth shifts that are everywhere less than 10 cm.

The BHTV logs probably have an azimuth accuracy of ±2° for the internal magnetometers (calibrated by Antares®) and ±2° for local deviation (measured by our on-ice reference magnetometer). Jarrard, Bücker et al. (this volume) confirm the reliability of the BHTV orientations by comparing average structural downdip azimuth for the shelf interval 100-789 mbsf based on BHTV (N66°E), dipmeter (N65°E), and regional seismic reflection profiles (N71°E).

BOREHOLE INDICATORS OF STRESS DIRECTION

The process of drilling a borehole causes a concentration of stresses around the borehole wall (*e.g.*, Zoback et al., 1985) and below the bit (*e.g.*, Lorenz et al., 1990). Because a borehole amplifies the far-field stress difference, very high compressive and absolute tensile stresses can occur around and beneath

the hole. If stresses are sufficient to cause the formation to fail in either tension or compression, analysis of the resulting failures can determine far-field, *in situ* stress directions.

Where the compressive stress concentration around the wall of the hole is larger than the rock strength, the rock fails and falls into the hole, forming a borehole breakout (Gough & Bell, 1981; Zoback et al., 1985). Breakouts form on opposite sides of a borehole. Their distinctive pattern of hole enlargements can be detected with 4-arm caliper logs if they are large enough. Breakouts smaller than 30° wide are common but not detectable even in 20-cm or larger holes; for HQ and NQ holes, pad widths preclude detection unless more than half of the borehole wall fails. Even when they are too small to be detected by caliper logs, breakouts are usually obvious on BHTV amplitude and traveltime logs. In vertical holes, breakouts occur at the azimuth of the least horizontal far-field stress. The occurrence (or non-occurrence) of breakouts and their widths can be used to quantify stress magnitudes (Zoback et al., 1985; Moos & Zoback, 1990).

Drilling-induced tensile wall fractures can form at the wall of a vertical borehole if the horizontal stress difference is quite large. These cracks are nearly vertical and on opposite sides of a borehole; their strikes parallel the direction of the far-field greatest horizontal stress. In vertical wells that are drilled with mud weights only slightly greater than the pore pressure, the formation of tensile cracks requires a large difference in the magnitudes of the horizontal stresses. Thus their presence or absence provides information to constrain stress magnitudes.

When mud weights are relatively high or the stress difference is large, stress concentration below the coring bit may be sufficiently high to induce tensile fractures below the bottom of the hole. At substantial depth, these generally form near the hole centre and are referred to as petal centre-line fractures (*e.g.*, Lorenz et al., 1990). At relatively shallow depth, these often form near the edges of the hole and are called core-edge fractures (Li & Schmitt, 1997; 1998). Both have characteristic features (*e.g.*, Moos et al., 2000; Paulsen et al., 2000). They can be differentiated from natural fractures because they do not cross the borehole and thus do not form complete sinusoids on BHTV images. The presence of these features in cores or BHTV images is an indication of large differential horizontal stresses. Their strike corresponds to the direction of the far-field greatest horizontal stress.

RESULTS

OBSERVED STRESS DIRECTION

The CRP-3 BHTV images provide 71 estimates of minimum horizontal stress direction. Petal centre-line and core-edge (PCL-CE) fractures, breakouts, and tensile fractures give generally similar results (Fig. 1). Figure 2 shows these data as a function of depth in the borehole.

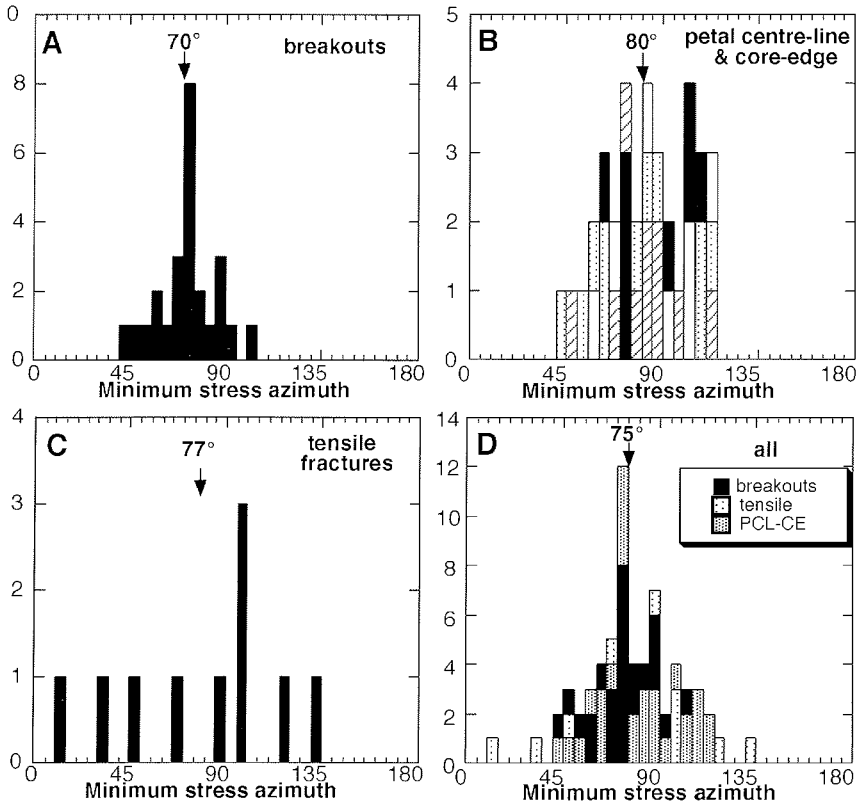

Fig. 1 - Histograms of estimates of minimum stress direction from breakouts (A), petal centre-line and core-edge (PCL-CE) fractures (B), tensile fractures (C), and combined data excluding possible natural fractures (D). Types of PCL-CE fractures in B are: confirmed in core (solid), possible natural fractures (white), ovals (diagonal lines), and other (dotted).

Borehole Breakouts

Borehole breakouts in the CRP-3 BHTV images have characteristic signatures of two vertical bands, ~180° apart and 25-30° in width, of very low amplitude and larger traveltime. Vertical extent of individual breakouts varies from 0.4 to 1.8 m. All of the observed breakouts occur in the bottom third of the hole, within the intervals 679-693 and 791-821 mbsf (Fig. 2). This lower interval corresponds closely to the 790-823 mbsf depth range of a doleritic breccia and conglomerate (Cape Roberts Science Team, 2000), and the breakouts are largely confined to interclast matrix, not doleritic boulders. Breakout azimuths are expected to parallel the direction of far-field, minimum horizontal *in situ* stress. Nearly all of the observed breakouts occur in well-defined pairs. Both azimuths were picked and displayed on figure 1 on a 0-180° scale, converting azimuths of 180-360° by subtracting 180°. The 25 breakout directions are tightly clustered at a mean azimuth of N70°E ± 6° (95% confidence limits).

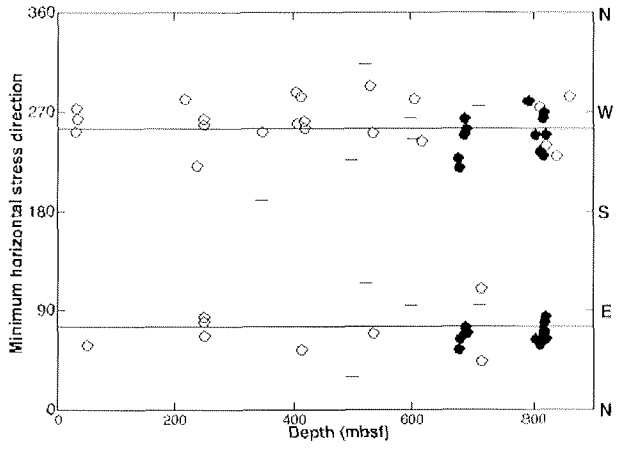

Fig. 2 - Estimates of minimum stress direction (excluding possible natural fractures) *vs.* depth. Symbols: breakouts (solid dots), petal centre-line and core-edge (open circles), and tensile cracks (-). Horizontal lines indicate mean orientation of minimum stress (75° and 255°, or N75°E and S75°W).

Petal Centre-line and Core-edge Fractures

Fractures that are described as petal centre-line (PCL) or core-edge (CE) within CRP cores (Cape Roberts Science Team, 1999, 2000; Wilson & Paulsen, this volume) also can be detected on BHTV images (Moos et al., 2000). Their diagnostic characteristics include an open-fracture signature, steep dip, clearly defined lower termination (often spalled), and limbs that become subvertical and disappear uphole. They strike perpendicular to the direction of minimum horizontal *in situ* far-field stress. Minimum stress direction can be picked as the down-dip termination azimuth and the average of the two limb orientations. Minimum stress directions based on these PCL-CE orientations are shown on figure 1 as a histogram with an azimuth scale of 0°-180°. The mean direction is N81°E, similar to but significantly greater than the N70°E azimuth of breakouts.

Ten BHTV fractures have a distinctively different shape than the typical half-sinusoid of PCL-CE fractures: they are ovals, 1-2 cm in height and 3-5 cm in width. This shape, which is similar to that of some core-edge fractures, may indicate drilling-induced fractures so near the edge of the bit that they barely intersect the borehole wall. These ovals have centre-point orientations of 70° and 268° (N70°E and S88°W), 198° apart and very similar to other PCL-CE orientations. We tentatively conclude that they are CE fractures and include them in the PCL-CE estimate of minimum stress direction, but we note that their inclusion does not significantly change the result.

The PCL-CE fractures, which are drilling-induced, cannot always be reliably distinguished from open, steep, natural fractures on BHTV images. Ideally, the latter form planar intersections with the borehole wall, evident as complete sinusoids on a BHTV image, whereas PCL-CE fractures form incomplete sinusoids that lack tops. However, CRP-3 BHTV image quality is often inadequate for detection of the complete sinusoidal signature of a natural fracture. To minimize the mispicking of natural fractures as PCL-CE fractures, we compared our listing of BHTV-based PCL-CE depths to two core-based lists: (1) depths of core-based PCL or CE fractures, and (2) depths of steep (>64°) natural fractures in cores.

Petal centre-line and core-edge fractures are common in CRP-3 HQ cores but relatively rare in the NQ cores (Cape Roberts Science Team, 2000; Wilson & Paulsen, this volume). In contrast, only one third of observed BHTV-based PCL-CE fractures are in HQ hole. BHTV images from the HQ hole are generally so poor that natural fractures, bedding, and clasts are rarely detectable, so the relative abundance of PCL-CE fractures in HQ *vs.* NQ intervals cannot be evaluated from BHTV data. Only 8 of the PCL or CE fractures identified in cores correspond in depth to BHTV-based PCL-CE fractures.

Most natural fractures within oriented CRP-3 cores have a NNE strike (Wilson & Paulsen, this volume). Consequently, the presence of natural fractures within our PCL-CE population would have the effect of biasing the mean azimuth of minimum stress toward a value higher than that measured with breakouts. Of the original 36 features picked as PCL-CE in BHTV images, 7 occur at the same depth as steep natural fractures in the cores. The PCL-CE average of 86° for those at the same depth as natural fractures is indeed intermediate between the 70° average from breakouts and the ~101° average dip azimuth (on a 0-180° scale) of natural fractures (Wilson & Paulsen, this volume), suggesting that bias is present. Excluding these data, the mean PCL-CE direction changes from N81°E to N80°E.

Tensile Fractures

Tensile fractures are evident in BHTV images as vertical open fractures that bisect the borehole, forming two narrow, low-amplitude, high-traveltime lines ~180° apart. Moos et al. (2000) show examples of tensile fractures from the CRP-2A BHTV log. Tensile fractures appear to be rare within CRP-3: only 6 such fractures, 1.1-4.4 m long, were detected. Tensile fractures are often associated with drilling events such as a bit change; within CRP-3, this generalization holds for all except the deepest pair of tensile fractures. The standard deviation of orientations is double that of breakout and PCL-CE azimuths, but the N77°E mean is similar (Fig. 1). Identification of tensile fractures in CRP-3 is less useful for stress direction than as a constraint on stress magnitude, as discussed in the next section.

STRESS MAGNITUDE

The presence (or absence) of wellbore failures (tensile wall fractures, borehole breakouts, and coring-induced tensile fractures) provides information on the magnitudes of *in situ* stresses (Moos & Zoback, 1990; Peska and Zoback, 1993). Moos et al. (2000) determined constraints on stresses in the interval penetrated by CRP-2A, based on the presence of tensile fractures and absence of breakouts. The information available in CRP-3 is more complete, as both breakouts and tensile cracks were observed in some intervals and not in others. Furthermore, a leakoff test was conducted at the HQ casing shoe, during the change from HQ to NQ drilling, providing a measure of least principal stress. The general approach used both here and in the previous study is to constrain the far-field stresses based on observations of wellbore failure using the elastic equations for stress concentrations around a vertical well. To apply this approach we use the fact that failure at the wall of a well occurs when the circumferential stress, $\sigma_{\theta\theta}$ exceeds the rock strength. For tensile failure, $\sigma_{\theta\theta}^{min} < -T$, where T is tensile strength; for compressive failure (breakouts), $\sigma_{\theta\theta}^{max} > C_{eff}$, where C_{eff} is effective strength.

In the case of tensile failure, we solve the elastic equation for the circumferential stress at the point where it is most tensile and exceeds the tensile strength. In the case where one principal *in situ* stress axis is vertical the equation, rewritten to solve for the maximum horizontal stress (S_{Hmax}), is:

$$S_{Hmax} \geq 3* S_{hmin} + T - P_p - P_{mud} - \sigma^{\Delta T} \quad (1)$$

The observation that tensile fractures both in this well and in CRP-2A were nearly axial to the vertical borehole supports our assumption that one principal stress is vertical. In order to solve this equation for S_{Hmax} it is necessary to measure or calculate the mud pressure (P_{mud}), pore pressure (P_p), and least horizontal stress (S_{hmin}). Mud pressure is the sum of the hydrostatic head induced by the static mud density and the pumping pressure, minus the pressure drop across the exit points within the bit: $P_{mud} = \rho_{mud} *g*h_{RKB} + P_{surface} - P_{drop}$, where ρ_{mud} is mud density and h_{RKB} is height of the mud column below the rig Kelly bushing. Pore pressure is $P_p = \rho_f *g*h_{bsl}$, where ρ_f is the formation fluid density and h_{bsl} is the height below sea level. The least horizontal stress can be determined from the shut-in pressure measured during an extended leakoff test. In order to use this value at depths other than the depth where the test was conducted, it is necessary to assume that the ratio $(S_{hmin}-P_p)/h_{bsl}$, computed from the shut-in pressure and the pore pressure at the shoe depth h_{bsf}, is a linear function of depth. Furthermore, we must assume that the shut-in test actually generated an hydraulic fracture which was shut in at the pressure corresponding to the least principal far-field stress, which — if less than the vertical stress as in this case - must be by definition S_{hmin}.

In the case of compressive failure of a vertical well, the width of breakouts (ϕ) can be related to S_{Hmax}, S_{hmin}, P_p, and P_{mud} as follows:

$$S_{Hmax} = \frac{\left(C_{eff} + 2P_p + \Delta P + \sigma^{\Delta T}\right) - S_{hmin}\left(1 + 2\cos 2\theta_b\right)}{1 - 2\cos 2\theta_b} \quad (2)$$

The effective strength (C_{eff}) increases as the mud pressure increases, and $\theta_b = 90 - \phi/2$. The thermally induced stress ($\sigma^{\Delta T}$) is assumed to be zero when the breakouts form, based on the fact that borehole temperatures after cessation of drilling were not much different from equilibrium (Bücker et al., this volume). $\Delta P = P_{mud} - P_p$.

In the case of no compressive failure, breakout width $\phi=0$ and therefore the term $2\cos 2\theta_b = -2$. In addition, $P_{mud}=P_p$ and therefore effective strength is equal to unconfined compressive strength (UCS). Consequently, equation 2 in the case where no breakouts occurred reduces to the simpler equation used in the CRP-2A analysis (Moos et al., 2000):

$$UCS \leq 3S_{Hmax} - S_{hmin} - 2P_p - \Delta P \quad (3)$$

Compressive and tensile failures within CRP-3 are assumed to occur at different stages of the drilling process: compressive failure occurs when the mud pressure is smallest and equal only to the static mud pressure, and tensile failure occurs when the mud pressure is greatest, during active pumping, when it is augmented by the excess pumping pressure. In this well it is also important when calculating the stresses that the presence of tensile cracks corresponds in two of the three cases to the depths of bit changes. Bit changes involve excess pumping, pump start-up and stopping pressures, and modest cooling which may overcome the finite tensile strength of the rock; all three processes enhance the likelihood of tensile cracks developing at these depths. One other tensile

fracture location is at the casing shoe, supporting the inference that the leakoff test actually did break down the formation and induce hydraulic fracturing. The observation that few tensile cracks occurred anywhere else supports the contention that the stress state is generally not conducive to tensile failure.

Rather than consider equations 1-3 individually, a better method is to present a plot of SHmax *vs.* Shmin with superimposed lines that indicate the combination of SHmax and Shmin that is consistent with the observed failures. We apply this graphical approach in figure 3, to calculate stresses at a true vertical depth of ~1030 m below sea level (mbsl), where tensile cracks developed at the point where a bit change was made. The lower blue line indicates the values of SHmax above which such failures would occur during pumping. The upper blue line indicates the conditions in the absence of pumping, which provides an upper bound on SHmax. We constrain the minimum stress using the initial shut-in pressure during the leakoff test at the HQ casing shoe (at a depth of 634 mbsl), which was between 1375 and 1405 psi (9.5-9.7 MPa). The corresponding Shmin gradient leads to a value at 1030 mbsl of approximately 2400 psi (16.6 MPa). The stress state consistent with these observations is indicated by the green triangle in figure 3, showing Shmin = 2400±100 psi (16.6 MPa), and SHmax = 3950±150 psi (27.2 MPa).

No breakouts occurred at this depth. In order for no breakouts to occur, rock compressive strength would need to be above approximately 6000 psi (41.4 MPa), which is consistent with laboratory-determined compressional velocities and densities (Jarrard, this volume). A short distance from this depth, breakouts did initiate within a sandstone at 979-993 mbsl. In order for these breakouts to occur, with widths ranging from 20 to 40 degrees, the rock strength only needs to be slightly less than above, within the range 5500 to 6000 psi (37.9-41.4 MPa), as shown on figure 3B. Measurements of unconfined compressive strength could provide a confirmation of the Shmin stress magnitude extrapolated from the leakoff test (for example, if Shmin were a bit lower, as indicated by the red triangle, the rock strengths consistent with the breakout observations would be lower).

A similar analysis can be conducted for the deeper interval 791-811 mbsf, a doleritic breccia in which breakouts developed within weak interclast matrix but not in stronger clasts. The absence of tensile cracks within this interval bounds the SHmax stress from above, resulting in overall stress estimates for this depth that are similar to those for the shallower zone. If rock strengths were known, the presence of breakouts in the weak rocks and absence in the stronger rocks could provide additional constraints on stress magnitudes at this depth as well.

Based on these analyses, stress magnitudes are strike-slip within CRP-3 (Figs. 3 & 4).

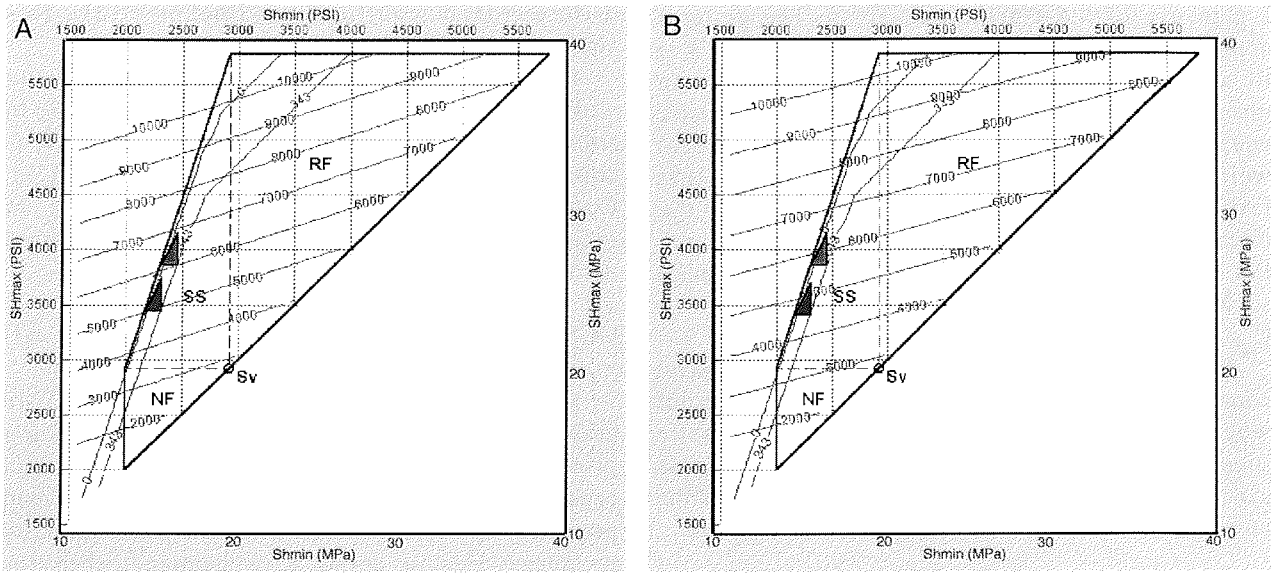

Fig. 3 - Constraints on stress magnitudes at a depth of approximately 1030 mbsl. The frictional strength polygon is black, red contours are conditions for breakouts (in psi), and blue contours are conditions for wall fractures (in psi). A: conditions that would cause breakouts to begin to form (wBO=0) while no circulation is occurring. The blue lines indicate bounding conditions to generate tensile cracks while pumping (excess pressure of 343 psi, or 2.4 MPa) and to avoid tensile cracks while not pumping (0 excess pressure). For a least stress of 2400±100 psi (16.6 MPa), the shaded zone shows the range of likely stresses if tensile cracks could form only during pumping, assuming that finite tensile strength is offset by modest cooling while pumping. The red lines indicate that no breakouts would form for these conditions if rock strengths are ~6500 psi (±500 psi to accommodate the uncertainty in SHmax) or ~44.8 MPa. B: the same shaded zone bounded by the same blue lines illustrates that breakouts 30-degrees wide could form for a rock strength of ~6000 psi (±500 psi to accommodate the SHmax uncertainty) or ~41.4 MPa. The green triangles are for a minimum stress consistent with the leakoff test, and the red triangles are for a somewhat lower minimum stress at this depth; both are within the strike-slip (SS) portion of the frictional strength polygon.

INTERPRETATION OF STRESS PATTERN

Stress magnitudes are strike-slip within CRP-3 (Figs. 3 & 4), in contrast to the normal to strike-slip stress state at CRP-2A (Moos et al., 2000). It is possible however that both results are correct, and that CRP-2A is in fact characterized by lower stresses than CRP-3. One possible explanation for the apparent difference is that the high stresses at both sites at these relatively shallow depths are a consequence of uplift and erosion which was much more pronounced at CRP-3 (~750 m) than at CRP-2 (~250 m). Uplift relieves the vertical stress but not the horizontal stresses, leading to high horizontal stresses at shallow depth relative to those at greater depth, with no change in stress orientation. Moos & Zoback (1993) documented this phenomenon using hydraulic fracturing measurements in wells in the eastern United States. Higher stress relief at CRP-3 than at CRP-2A is also suggested by core velocity measurements: velocity sensitivity to pressure is significantly higher at CRP-3 than at CRP-1 and CRP-2A, attributable to either rebound or microcracks at CRP-3 (Jarrard, this volume).

The occurrence of stress-direction indicators in CRP-3 BHTV images shows both similarities and differences to those reported by Moos et al. (2000) for CRP-2A, 2 km away. Tensile fractures were detected but rare at both sites. PCL-CE fractures are common at both sites but much more abundant at CRP-2A (Paulsen et al., 2000; Cape Roberts Science Team, 2000). In an effort to improve hole conditions, drillers used consistently lower mud weights at CRP-3 than those employed for CRP-2A (Cape Roberts Science Team, 2000). The resulting decrease in hydraulic head is less likely to induce PCL-CE fractures. Breakouts are detected at CRP-3 but not at CRP-2A, probably because of the shallower depth of the CRP-2A BHTV log. The CRP-2A BHTV log ended at 444 mbsf, whereas all breakouts at CRP-3 occurred below 679 mbsf. Dipmeter logging, which extended to 623 mbsf at CRP-2A and 902 mbsf at CRP-3, detected no breakouts at either site. The combination of relatively large dipmeter pads and small-diameter hole permits detection only of very wide breakouts.

The combined orientations of breakouts, PCL-CE fractures (excluding possible natural fractures), and tensile fractures at CRP-3 provides an overall average determination of N75.5°E ± 5.5° (95% confidence limits) for minimum horizontal stress direction. Breakouts, which we consider to be the most accurate indicators of stress direction for CRP-3, have an average azimuth of N69.6°E ± 5.7°. These estimates are compatible with the N77°E minimum stress direction determined by Moos et al. (2000) from CRP-2A BHTV images, based mainly on PCL-CE orientations.

Local topography can dominate the horizontal stress pattern of shallow wells, because of lack of lateral confining pressure from the topographic low; in an extreme case, slumping results. The net topographic effect is to generate a minimum stress direction perpendicular to topographic contours. CRP-2A and CRP-3 penetrate seafloor with a local topographic slope of ~2° to the west. The minimum horizontal stress directions for both sites are significantly different from the S82°E prediction for a

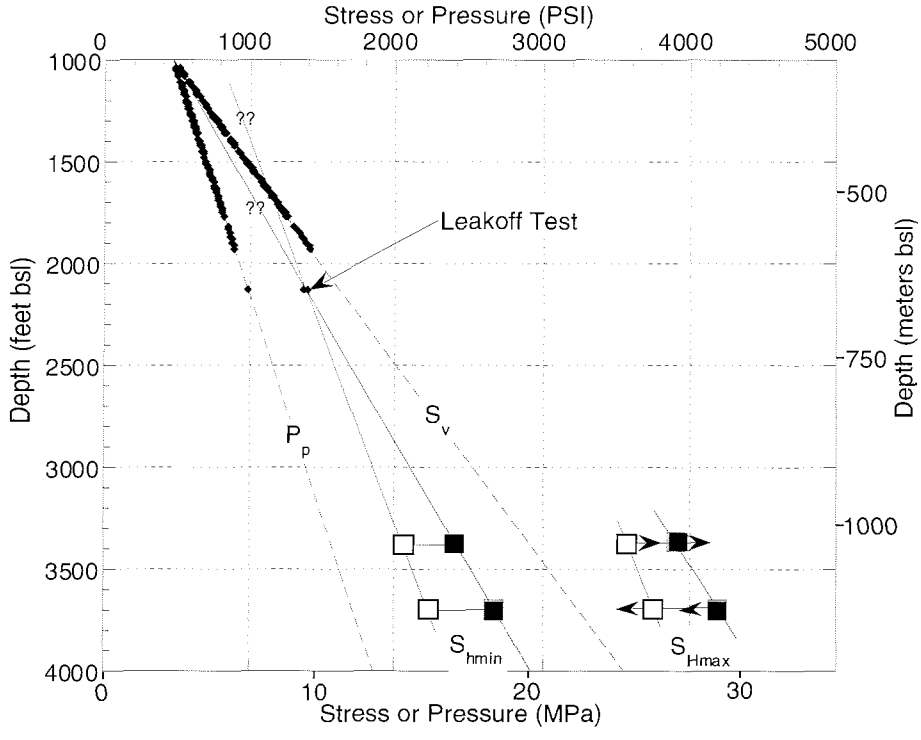

Fig. 4 - Stress analysis results. S_v is computed from integration of laboratory measurements. P_p is computed assuming a gradient of 0.465 psi/ft (0.001 MPa/m). The two lines for Shmin are (a) assuming that it is equal to S_v at the sea floor, and (b) assuming that it has a finite value at the sea floor. Both assumptions are reasonable, but a finite value is more likely. SHmax values are constrained by the following: (1) observations of tensile cracks at 1010 m bsl (where excess pumping may have contributed to their formation) and no tensile fractures at immediately below that depth and at approximately 1105 m bsl, and (2) the assumed projection of the Shmin gradient to those depths.

topographically dominated local stress field. Furthermore, the depths of most of the stress directions from CRP-2A are greater than the deepest portion of the adjacent topographic low, 4 km away, and the depths of virtually all of the CRP-3 stress directions are much deeper than the topographic low, so a topographic effect appears to be unlikely.

Presence of a significant topographic effect at CRP-3 would generate a downhole rotation of minimum stress direction, because the net stress is a sum of topographic and tectonic effects, and the topographic effect decreases downhole. In contrast to this prediction, the CRP-3 minimum-stress directions exhibit no evidence of systematic changes as a function of depth (Fig. 2). The uniformity of direction, throughout both Tertiary and Devonian intervals and both across and within faults (~260 mbsf, ~539 mbsf, and 790-802 mbsf), suggests that it is truly a representative, far-field stress direction rather than one biased by local stress gradients.

The N75°E modern minimum stress direction is very similar to several palaeostress indicators. Early Oligocene (or latest Eocene?) rifting of this region presumably involved extension approximately perpendicular to the modern coastline, towards ~N72°E (Cape Roberts Science Team, 1999). Oligocene and Early Miocene growth faulting and tilting had similar orientations: dipmeter data indicate downdip azimuths of N75°E at CRP-2A (Jarrard et al., 2000) and N65°E at CRP-3 (Jarrard, Bücker et al., this volume). The stress history of this region is more complex than extension uniformly toward ~N75°E, however. Hamilton et al. (1998) have mapped a variety of fault orientations based on seismic data, none of which (including the major boundary fault) are perpendicular to ~N75°E. Wilson (1995) has documented transtension and NNE-ENE striking fractures onshore Cape Roberts. Furthermore, the dominant fracture strike observed in oriented cores from CRP-3 is NNE (Wilson & Paulsen, this volume).

ACKNOWLEDGEMENTS -This research was supported by the National Science Foundation (OPP-9527319, OPP-9527412, and OPP-9517394). We thank Alex Pyne for optimizing logging conditions and providing information on drilling parameters.

REFERENCES

Bücker C.J., Jarrard R.D. & Wonik T, 2001. Downhole temperature, radiogenic heat production, and heat flow from the CRP-3 drillhole, Victoria Land Basin, Antarctica. This volume.

Cape Roberts Science Team, 1999. Studies from the Cape Roberts Project, Ross Sea, Antarctica, Initial Report on CRP-2/2A. *Terra Antartica*, **6**, 1-173.

Cape Roberts Science Team, 2000. Studies from the Cape Roberts Project, Ross Sea, Antarctica, Initial Report on CRP-3. *Terra Antartica*, **7**, 1-209.

Gough D. I. & Bell J. S., 1981. Stress orientations from oil well fractures in Alberta and Texas. *Can. J. Earth Sci.*, **18**, 1358-1370.

Hamilton R.J., Sorlien C.C., Luyendyk B.P., Bartek L.R. & Henrys S.A., 1998. Tectonic regimes and structural trends off Cape Roberts, Antarctica. In: Barrett P.J. & Ricci C.A. (eds.), Studies from the Cape Roberts Project, Ross Sea, Antarctica – Scientific Report of CRP-1, *Terra Antartica*, **5**, 261-272.

Jarrard R.D., Brink J.D., Bücker C., Wonik T., Wilson T.J. & Paulsen T.S., 2000. Bedding dips in CRP-2A, Victoria Land Basin, Antarctica. *Terra Antartica*, **7**, 261-270.

Jarrard R.D., 2001. Petrophysics of core plugs from CRP-3 drillhole, Victoria Land Basin, Antarctica. This volume.

Jarrard R.D., Paulsen T.S. & Wilson T.J., 2001. Orientation of CRP-3 core, Victoria Land Basin, Antarctica. This volume

Jarrard R.D., Bücker C.J., Wilson T.J. & Paulsen T., 2001. Bedding dips from the CRP-3 drillhole, Victoria Land Basin, Antarctica. This volume

Li Y. & Schmitt D.R., 1997. Well-bore bottom stress concentration and induced core fractures. *AAPG Bulletin*, **81**, 1909-1925.

Li Y. & Schmitt D.R., 1998. Drilling-induced core fractures and in situ stress. *J. Geophys. Res.*, **103**, 5225-5239.

Lorenz J.C., Finley S.J. & Warpinski N.R., 1990. Significance of coring-induced fractures in Mesaverde core, northwestern Colorado. *AAPG Bull.*, **74**, 1017-1029.

Moos D., Jarrard R.D., Paulsen T.S., Scholz E. & Wilson T.J., 2000. Acoustic borehole televiewer results from CRP-2/2A, Victoria Land Basin, Antarctica. *Terra Antartica*, **7**, 279-286.

Moos D. & Zoback M. D., 1990. Utilization of observations related to wellbore failure to constrain the orientation and magnitude of crustal stresses: Application to continental, DSDP and ODP boreholes. *J. Geophys. Res.*, **95**, 9305-9325.

Moos D. & Zoback M. D., 1993. Near-surface, "thin skin" reverse faulting stresses in the Southeastern United States. *Intl. J. Rock Mech. Min. Sci. & Geomech. Abstr.*, **30**, 965-971.

Paulsen T.S., Wilson T.J., Moos D., Jarrard R.D. & Wilson G.S., 2000. Orientation of CRP-2A core. *Terra Antartica*, **7**, 271-278.

Peska P. & Zoback M.D., 1995. Compressive and tensile failure of inclined well bores and determination of in situ stress and rock strength. *J. Geophys. Res.*, **100**, 12791-12811.

Richardson R.M., 1992. Ridge forces, absolute plate motions, and the intraplate stress field. *J. Geophys. Res.*, **97**, 11739-11748.

Wilson T.J., 1995. Cenozoic transtension along the Transantarctic Mountains - West Antarctic Rift boundary, Southern Victoria Land, Antarctica. *Tectonics*, **14**, 531-545.

Wilson T.J. & Paulsen T.S., 2001. Fault and fracture patterns in CRP-3 core, Victoria Land Basin, Antarctica. This volume

Zemanek J. Glenn E.E., Norton L.J. & Caldwell R.L., 1970. Formation evaluation by inspection with the borehole televiewer. *Geophysics*, **35**, 254-269.

Zoback M. D., Moos D., Mastin L. & Anderson R. N., 1985. Wellbore breakouts and in-situ stress. *J. Geophys. Res.*, **90**, 5523.

Zoback M.L., 1992. First- and second-order patterns of stress in the lithosphere: the World Stress Map project. *J. Geophys. Res.*, **97**, 11703-11728.